Laser-based Soldering Technique for Hermetical Sealing of the Calibration Target for the Exomars' Raman Instrument

Thomas Burkhardt[1], Michael Seifert[1], Pol Ribes[1,2], Nicolas Lange[1], Guillermo Lopez-Reyes[3], Andoni Moral-Inza[4] and Antonio Sansano[3]

[1]*Fraunhofer Institute for Applied Optics and Precision Engineering IOF, Albert-Einstein-Str. 7, 07745 Jena, Germany*
[2]*Institute of Applied Physics IAP, Friedrich-Schiller University Jena, Max-Wien-Platz 1, 07743 Jena, Germany*
[3]*Unidad Asociada UVA-CSIC-CAB, Universidad de Valladolid, Parque Tecnológico Boecillo, 47151 Valladolid, Spain*
[4]*Instituto Nacional del Tecnica Aerospacial INTA, Ctra Ajalvir Km4, 28850 Torrejón de Ardoz, Spain*

Keywords: ExoMars Raman Laser Spectrometer, Calibration Target, Laser-based Soldering, Solderjet Bumping, Hermetical Sealing.

Abstract: We propose the laser-based Solderjet Bumping as a full inorganic joining technique for the hermetical sealing of a possible calibration target container for the ExoMars Raman Laser Spectrometer. This technique allows the adhesive free bonding in a flux free and localized soldering process. We show a finite elements analysis based optimization of a soldering adapted design for the calibration target container. Current experimental results document hermetical sealing of a stainless steel tube with BK7 and D263 windows with a helium leakage rate down to $5 \cdot 10^{-6}$ mbar·l·s^{-1}.

1 INTRODUCTION

1.1 Motivation

In 2018 ESA/Roscosmos will launch the ExoMars Rover mission. The main target of this mission is to study the Martian environment and to test new technologies paving the way for a possible Mars return mission in the 2020s. Raman spectroscopy is a tool for the chemical and structural identification of (sub-)surface materials and organic analysis to address the scientific objective of the Pasteur payload to search for evidence of past and present life on Mars (Rull Pérez and Martinez-Frias, 2006; Escudero et al., 2008). The Raman Laser Spectrometer (RLS) is together with the MicrOmega (IR spectrometer) and the Mars Organic Molecule Analyzer (MOMA) part of the rover's analytical laboratory drawer (ALD). They are key exobiology experiments on the ExoMars rover mission to examine the chemical composition of geological samples acquired from depths of up to two meters, where possible organic molecules may be protected from destructive cosmic radiation and/or oxidative chemical reactions (Arevalo et al., 2015). For calibration of the RLS on board the rover, a calibration target (CT) will be included. This allows periodic calibration of the instrument for high precision and to evaluate the health of the system during the mission (Sansano et al., 2014). During each analysis (several hours), at least 20 spectra at different points of the sample will be acquired. Before each experiment cycle, the CT will be used to assess the calibration status of the whole instrument in an end-to-end calibration, including the laser optical head, harness, spectrometer, and electronics. There will be at least 22 experimental cycles, each of them with a different sample.

As the CT will be located in the ultra clean zone (UCZ) of the ALD, the CT container is to be suitably sealed. It needs to comply with planetary protection requirements to prevent biological contamination of Mars to preserve its pristine nature and also to prevent the corruption of the mission's experiments. To achieve this ambitious protection and contamination control COSPAR Cat IVb classification measures are implemented to avoid the terrestrial contamination of the analyzed samples. According to Richter et al. (2015) this addresses the whole Sample Processing and Distribution Subsystem (SPDS) and includes the pressurized UCZ (pressurized during launch, transfer, and landing), sterilization of the ALD sample chain, ultra

Burkhardt, T., Seifert, M., Ribes, P., Lange, N., Lopez-Reyes, G., Moral-Inza, A. and Sansano, A.
Laser-based Soldering Technique for Hermetical Sealing of the Calibration Target for the Exomars' Raman Instrument.
DOI: 10.5220/0005653200550061
In *Proceedings of the 4th International Conference on Photonics, Optics and Laser Technology (PHOTOPTICS 2016)*, pages 57-63
ISBN: 978-989-758-174-8

cleaning of the ALD sample chain components, and integration of the hardware in a high cleanliness environment.

1.2 Solderjet Bumping Technique

We propose the laser-based Solderjet Bumping as a full inorganic joining technique for the hermetical sealing of a possible CT container candidate. It allows the adhesive free bonding of heterogeneous materials, e.g. metals with glass, in a flux free process. The soldered assembly is therefore completely free of undesired organic compounds. Furthermore the solder joints are able to withstand high thermal loads during sterilization and high energetic radiation, e.g. cosmic radiation during transfer of the lander to and its mission on Mars.

Solderjet Bumping (Figure 1) is a laser-based soldering process that is especially well suited for the joining of optical components made of fragile and/or brittle materials like glasses or ceramics. Spherical solder preforms that consist of soft solders alloys, e.g. tin-based lead-free solders or eutectic gold-tin, are used in a diameter range of 60 µm to 760 µm. These spheres are transferred from a reservoir to a placement capillary next to the joining geometry of the components to be bonded together. After positioning, the material is molten by a fiber-coupled, infrared laser pulse and jetted out of the capillary. Nitrogen is used as an inert gas flow. The liquid solder droplets account for a very good thermal contact of the alloy with the components.

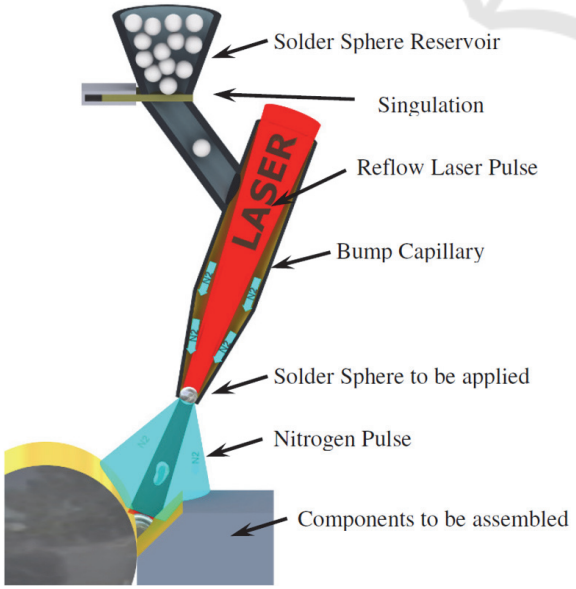

Figure 1: Solderjet Bumping operation principle (Beckert et al., 2010).

We have demonstrated the versatility of this technique for the high accuracy packaging of photonic micro-systems (Beckert et al., 2010). Hermetical sealing of biomedical devices (Beckert et al., 2011) and the vacuum compatibility of soldered assemblies for the use in electron beam lithography (Burkhardt et al., 2011) have been proven. We presented Solderjet Bumping for optical instrumentation in aerospace applications (Burkhardt et al., 2015). The technique has been used for the manufacturing of a compact and robust, solid-state laser for the ExoMars mission and was tested at thermal and radiation (proton and gamma) loads (Ribes et al., 2015).

2 DESIGN AND OPTIMIZATION

2.1 Requirements

The CT consists of a cylindrical, stainless steel container of 5..6 mm diameter. A cavity in the container will be covered by a thin glass window, fused silica and BK7 will be discussed as candidates. The window will contain the calibration sample and needs therefore to be hermetically sealed to prevent organic molecular contamination of the UCZ. A mixture of powdered standard compounds (both organic and inorganic) with a known spectral Raman response covering the entire spectral range will be filled in this sealed envelope (Sansano et al., 2014). Regarding the calibration sample both an encapsulated mixture – a pill with diameter 4 mm and thickness 3 mm – and non-encapsulated powder are discussed. The main laser characteristics during calibration are continuous operation at 532 nm, with 50 mW optical output power that is focused on 50 µm diameter spot on the sample.

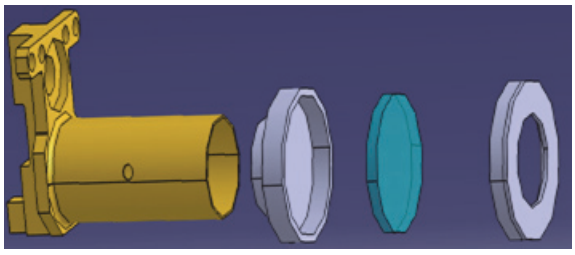

Figure 2: Design proposal of CT holder elements (Sansano et al., 2014).

BK7 is selected over its radiation resistant counterparts (e.g. BK7G18) for multiple reasons. These include availability as thin glass sheets and manufacturability to the designed shape, its

thermomechanical properties with respect to the stainless steel receptacle. A trade-off in BK7's preferability for space applications in terms of radiation damage is accepted as radiation obscuration is well characterised for ionising and non-ionising doses is accepted for a known Raman signature of the material. Given that the window of the CT container would be placed very deep inside the ALD of the rover the expected radiation levels should not to be a major concern for the obscuration of the window.

Due to obvious weight restrictions the maximum required weight is 9 g with a further decrease to 4 g during STM (structural and thermal model) design. Figure 2 shows the design proposal of a CT and holder elements as a basis for the design considerations of a CT suitable for Solderjet Bumping. The required envelope, including the support, is the one contained in a parallelepiped of 13×26.3× 10.9 mm³.

The thickness of the glass window is required to be 100 µm maximum. A maximum height difference between the top surface of the window and the solder joint of 50 µm is permitted. This is necessary for the CT to be within the agreed envelope for avoiding any interference with the rover's carrousel powdered sample flattener.

2.2 Design and FEA Results

Based on the requirements of the CT a model of the receptacle is developed to simulate and evaluate thermomechanical, shock, acceleration, and vibrational loads. Different solder joint geometries are investigated and optimized according to the results of the finite elements analysis (FEA).

Figure shows the model and initial dimensions used in FEA simulations and optimization. The simplified model omits the enclosed powder sample as thermomechanical simulations will not be affected as there is no transfer of forces or momenta. In dynamic simulations the powder would act as an additional mass, dampening the response behavior of the whole receptacle thus the simulated empty system shows the worst case results.

Details of the solder joint showing the receptacle, the window, and the solder itself are depicted in Figure 4. A gap of 100 µm between receptacle and window is assumed to accommodate for manufacturing tolerances. Initial simulations assumed the shown 600 µm width and 100 µm height of the solder joint to bridge this gap. These values could be achieved using a solder sphere diameter of 400 µm, overlapping placement, and typical, experimentally validated wetting behavior.

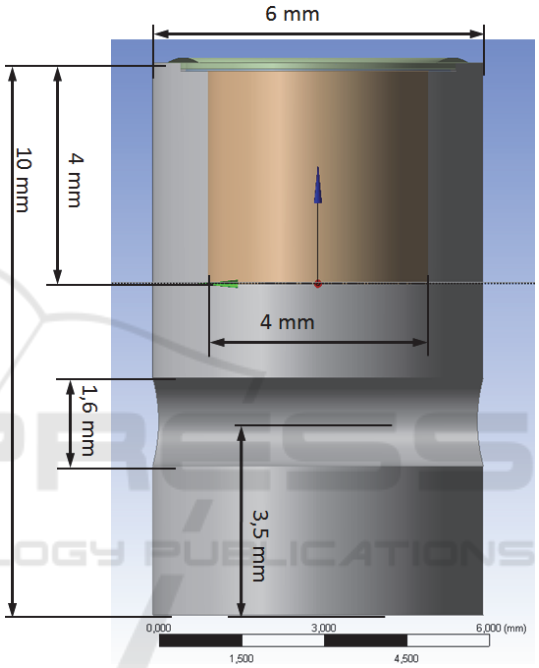

Figure 3: Simulated receptacle with dimensions.

Material parameters used for the simulations for the stainless steel, the window (both fused silica and BK7), and the solder alloy (SAC305 = Sn3Ag0.5Cu) are listed in Table 1. The equivalent Von-Mises stresses as well as the total deformation are evaluated in all three individual parts: receptacle, glass window, and solder ring.

Table 1: Material parameters used for FEA simulations.

	Stainless Steel	Fused Silica	BK7	SAC305
Young's Modulus / GPa	193	73.2	82	44
Poisson's Ratio	0.31	0.17	0.21	0.36
Density	7.75	2.02	2.2	7.4
CTE / $10^{-6}\cdot K^{-1}$	17	0.56	7.1	22.4
Thermal Conductivity / $W\cdot m^{-1}\cdot K^{-1}$	15.1	1.4	1.1	56.3
Specific Heat / $J\cdot kg^{-1}\cdot K^{-1}$	480	750	858	283
Yield Strength / MPa	207	N/A	N/A	N/A
Ultimate Tensile Strength / MPa	586	50	63.5	45

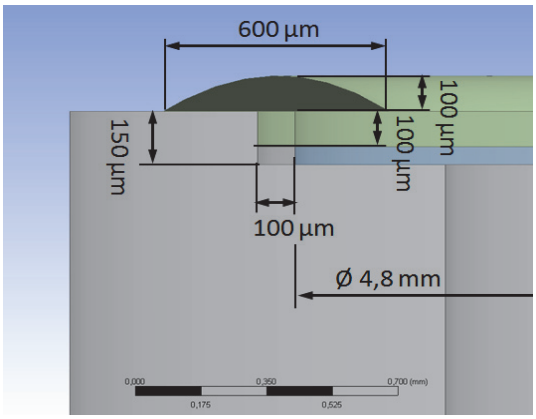

Figure 4: Detail of the solder joint of the receptacle with initial design values.

2.3 Design Optimization

2.3.1 First Iteration

First thermomechanical simulations according to the model presented in Figure 3 and Figure 4 and a temperature range from -60 °C to +130 °C show maximum stresses in the solder of 229 MPa and in the window (fused silica) of 133 MPa. Both significantly exceed the ultimate tensile strength (UTS) of these materials (see Table 1) which is mainly caused by the large mismatch of the coefficient of thermal expansion. Static structural acceleration, transient structural shock, harmonic load, and random vibration simulation all show acceptable stress levels with a minimum safety factor of 8.5. The results are not presented here as the model had to be refined to improve the thermal behavior.

To avoid damage to the solder and window a design optimization is investigated. Besides a reduction in differential thermal expansion (DTE) a few concepts are followed and simulated accordingly. A promising approach is a changed gap between the components, a thicker glass material, a cylindrical geometry with reduced stiffness at the top of the receptacle, and a change in geometry of the solder joint.

A refined geometry with reduced stiffness at the top of the receptacle minimizing DTE to relief stress uses a reduced wall thickness of the cylinder of 0.5 mm compared to initial 1 mm. The gap between cylinder wall and window is decreased – a measure that requires tighter tolerances for the experimental samples. Furthermore the solder joint size is decreased both in width and thickness, which will experimentally be realized by using smaller solder spheres (diameter 100 µm or 150 µm).

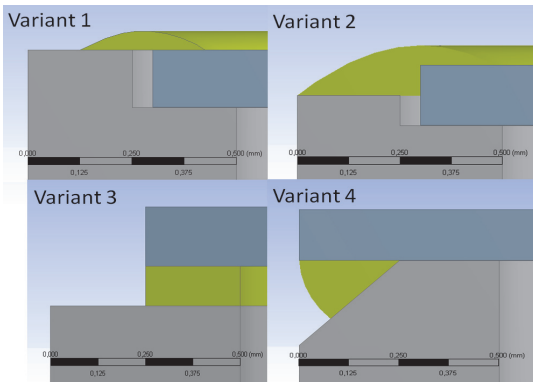

Figure 5: Refined geometries of iteration 1.

In addition to the changed geometry the simulations were done with Fused Silica as well as BK7 as glass material. The advantage is the significantly increased CTE of BK7, lowering the DTE with respect to the steel tube, and the increased UTS compared to Fused Silica (see Table 1). Four geometries are investigated as shown in Figure.

Table 2: Maximum Von-Mises stresses in solder joint and glass window for thermal load of 130 °C and calculated minimum safety factors (FS denotes Fused Silica).

Type	Solder Stress / MPa	Solder Safety Factor	Window Stress / MPa	Window Safety Factor
V1, FS	378	0.12	240	0.21
V1, BK7	232	0.19	162	0.39
V2, FS	381	0.12	155	0.32
V2, BK7	258	0.18	109	0.58
V3, FS	209	0.22	158	0.32
V3, BK7	138	0.33	109	0.58
V4, FS	1380	0.03	269	0.19
V4, BK7	881	0.05	183	0.35

Table 2 lists the resulting maximum Von-Mises stresses for a thermal load of 130 °C and the respective minimum safety factors using UTS values as listed in Table 1. While the stresses in the solder and the glass window still significantly exceed the materials UTS an improvement due to the use of BK7 can be observed. This is traced back to the CTE which is 12 times higher for BK7 than for Fused Silica and the 13.5 MPa higher UTS. Variants 1, 2, and 4 show stress distributions with very localized peaking that indicate a potential improvement by refining the geometry.

2.3.2 Second Iteration

Based on the results for the four variants discussed in the previous sub subsection, the geometries for three variants are further refined and simulated again under the same conditions. Due to overall low

stresses variant 2 will not be refined further. Variants 1, 3 and 4 on the other hand are showing potential for further improvements and are therefore further investigated. In addition plasticity of the solder alloy is added to the model to create a more realistic representation. Figure 6 shows the improved geometries 1.1 and 4.1 with rounded edges to minimize stress. Variant 3.1 is similar to variant 3 as depicted in Figure 5 with a decreased solder layer thickness of 50 µm. Table 3 lists the maximum Von-Mises stresses for a thermal load of 130 °C respective minimum safety factors using UTS values as listed in Table 1 for the improved designs both for elastic and plastic modelling of the solder.

Table 3: Maximum Von-Mises stresses in solder joint and glass window for thermal load of 130 °C and calculated minimum safety factors for second design iteration. Calculations using plasticity are marked with an asterisk.

Type	Solder Stress / MPa	Solder Safety Factor	Window Stress / MPa	Window Safety Factor
V1.1	238	0.2	101	0.6
V1.1 *	51	0.9	75	0.8
V3.1	163	0.3	110	0.6
V3.1 *	48	0.9	85	0.8
V4.1	259	0.2	167	0.4
V4.1 *	52	0.9	113	0.6

The plasticity allows the solder alloy to balance and even out the occurring stresses in the components, thus increasing the minimum stresses but decreasing the maximum stresses. As a result the minimum safety factors increase and the maximum safety factors decrease (note that only minimum safety factors are listed in Table 3). Considering these changed stress and safety factor conditions, variant 1.1 (as calculated with plasticity) shows the optimal compromise of a sufficiently high minimum and maximum safety factor in all three components. In addition variant 1.1 has the best prerequisites for the technological realization in contrast to the more complicated solder process required for variant 3.1 and 4.1. With refining the geometries of the three chosen variants the occurring stresses could be further reduced. By introducing the plasticity to material formulation of the solder alloy said stresses were successfully smoothed and balanced in all three components, reducing the extreme values.

All evaluations were done with the absolute maximum stress values that occur at each component representing the worst case. The average stress in each component is expected to be significantly lower and indicates the possible use of soldering the proposed assemblies. Transient and dynamic mechanical load cases were simulated for the optimized models and show minimum safety factors of 14.5 and a first Eigenfrequency of 50 kHz. Considering these mechanical loads an assembly of the CT using Solderjet Bumping seems feasible.

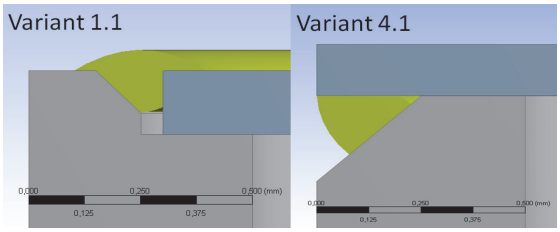

Figure 6: Refined geometries of iteration 2.

3 EXPERIMENTAL RESULTS

As suggested by the results variants 1 and 1.1 are the most promising candidates for successful soldering. Furthermore variants 3.x and 4.x require significantly more elaborate handling equipment. Experimental verification as reported in this paper is therefore using samples made according to design variants 1 and 1.1.

Due to commercial availability one batch of experiments was conducted using D263 glass which shows similar thermomechanical properties as BK7 especially an equivalent CTE but is available as thin sheet glass (thickness 145 µm). These samples were prepared at IOF from sheets. The second batch of experiments was done using BK7 windows with a thickness of 175 µm. These samples were also prepared at IOF from sheets. A third batch of BK7 samples was procured from Laser Optex, China, with a thickness of 150 µm ± 2 µm.

Both the windows and the stainless steel cylinder are covered by a solderable thin film metallization. It is provided by physical vapor deposition and consists of three layers: titanium, platinum, and gold. The metallization system has an overall thickness of approx. 500 nm. Titanium acts as adhesion promoter, platinum as diffusion barrier, and the wettable, non-oxidizing gold finish supports the required flux-free processing to achieve a clean solder joint. (Banse et al., 2005) reported this system among others as a suitable and well adhering metallization for glass materials.

3.1 Soldering and Optical Inspection

Soldering is conducted using a solder sphere diameter of 100 µm and 150 µm according to the optimized design of the solder joints. Relevant

parameters for the laser-based Solderjet Bumping are the reflow energy governed by laser pulse width and laser current. Using glass slides these parameter sets are evaluated to find proper wetting of the solder in the substrate while preventing damage to the glass. The latter is especially an issue with soldering as thermal shock can cause cracks to form and propagate in the glass leading to failures of the bond. We found suitable parameters as listed in Table 4. The increased necessary energy corresponds well to increased solder volume and mass (approx. factor 3.4). These investigations show the limited parameter space for soldering thin sheet glass and the possible issues with soldering near the edges of said glass sheets.

Table 4: Laser reflow parameter sets.

Solder Sphere Diameter / µm	Laser Current / mA	Laser Pulse Width / ms	Puls Energy / mJ
100	1500	1	7.4
150	1700	2.4	22.5

Glass windows are inserted in the stainless steel tube, adjusted for an even and symmetrical distribution of the gap around the circumference, and kept in place by application of vacuum. A bond height – the distance of the Solderjet's placement capillary to the soldered components – of 350 µm for 100 µm solder spheres and 550 µm for 150 µm is used. These distances are selected to provide undisturbed application of the liquid solder droplet with minimized deviation of placement accuracy.

Soldering is a sequential process to subsequently place multiple overlapping bumps. We investigated different placement strategies, e.g. an interlaced placement scheme and multiple turns to accommodate for a larger gap between window and tube due to issues with tolerances. We did not find a significant influence of the placement scheme on leakage rate as long as a completely closed solder joint is achieved and no holes are observable by visual inspection. Placement of solder droplets is done in an automated system using a vision system and a circular fit to adjust the machine's tool path with the outline of the sample. A total of 288 bumps per turn are placed at a solder sphere diameter of 100 µm and 232 bumps per turn for 150 µm preform diameter, respectively.

Figure 7 shows a sealed CT filled with mock-up sample compound. The total weight of the sample is less than 2 g within the STM design limit. A total height of the solder joint of less than 50 µm is achieved using solder droplet diameters of 100 µm.

Figure 8 shows a top view photomicrograph of the sample and the solder joint. It illustrates clearly the regular and clean overlapping placement of multiple solder droplets in the bond zone to provide proper mechanical fixation of the window as well as hermetical sealing.

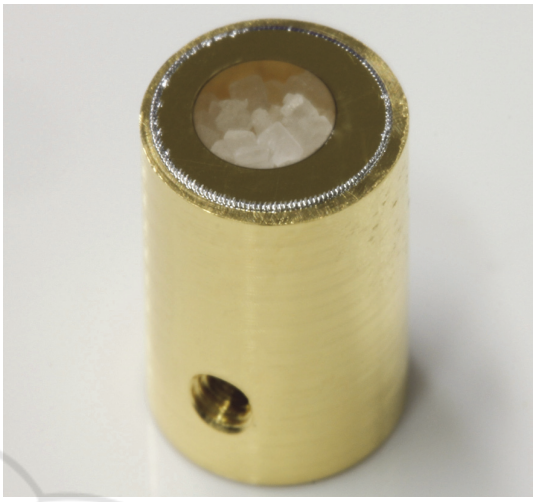

Figure 7: Sealed calibration target filled with mock-up sample compounds and BK7 window.

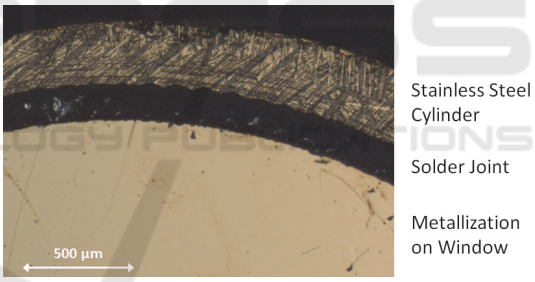

Figure 8: Photomicrograph of solder joint.

3.2 Helium Leakage Testing

For measuring the leakage rate a Leybold Inficon UL200 was used. Minimum detectable leakage rate in vacuum mode is $5 \cdot 10^{-11}$ mbar·l·s^{-1}. For testing, the cylinders were fixed with an adapter to the leak tester and evacuated. The soldered windows were then sprayed with Helium and the leakage rate was measured.

For batch one using D263 glass, thickness 145 µm, out of seven samples we found one sample exceeding $5 \cdot 10^{-6}$ mbar·l·s^{-1}, three samples exceeding 10^{-4} mbar·l·s^{-1}, and one sample exceeding 10^{-2} mbar·l·s^{-1}.

With BK7 glass, thicknesses of 175 µm and 150 µm, out of eight samples we found two samples exceeding 10^{-4} mbar·l·s^{-1}, two samples exceeding

10^{-3} mbar·l·s^{-1}, and three sample exceeding 10^{-2} mbar·l·s^{-1}. A major issue is the surface quality of the window's edges. We observe the formation of micro-cracks during soldering which in turn significantly increase leakage rate. While the procured windows show a very narrow thickness tolerance, the edges are not polished and therefore susceptible to crack induced by thermal shock.

4 CONCLUSIONS

We have shown the hermetical sealing of a multi-material assembly for the possible use as a calibration target container for the ExoMars Raman Laser Spectrometer. Proof-of-concept samples made of stainless steel and D263 achieved leakage rates of $5 \cdot 10^{-6}$ mbar·l·s^{-1}. The bonding is completely inorganic and therefore suitable for high cleanliness and contamination free applications, e.g. under COSPAR planetary protection requirements.

A FEA tool chain and models were set up for optimization of joint geometries and were used to provide appropriate design recommendations for minimized stresses. Mechanical and thermomechanical load cases were investigated by numerical simulations. A minimized differential thermal expansion is found to be necessary to achieve acceptable stress levels in the solder joint.

Although the presented design of the container and therefore the proposed bonding will not be used for the RLS CT the results show the adequacy of Solderjet Bumping for hermetical sealing and aerospace applications. The development activities continue and the technology is kept as a backup plan for the ExoMars RLS CT.

Further improvements of leakage rate and reduced failures during bonding are expected with optimized sample geometries, improved surface quality of the windows' circumferential side faces, and adapted tolerances between receptacle and window. A goal would be to achieve a helium leakage rate better than 10^{-8} mbar·l·s^{-1}. Experimental qualifications based the mechanical and thermal load cases considered for the numerical optimizations have to be conducted with further samples.

ACKNOWLEDGEMENTS

The authors gratefully acknowledge funding from MINECO, Spain, through project ESP2013-48427-C3-2-R.

REFERENCES

Arevalo, R., Brinckerhoff, W., van Amerom, F., Danell, R., Pinnick, V., Xiang Li, Getty, S., Hovmand, L., Grubisic, A., Mahaffy, P., Goesmann, F., Steininger, H., 2015, Design and demonstration of the Mars Organic Molecule Analyzer (MOMA) on the ExoMars 2018 rover, in: *Aerospace Conference, 2015 IEEE*.

Banse, H., Beckert, E., Eberhardt, R., Stöckl, W., Vogel, J., Laserbeam soldering– a new assembly technology for micro optical systems, *Microsyst. Technol. 11, 186–193 (2005)*.

Beckert, E., Burkhardt, T., Hornaff, M., Kamm, A., Scheidig, I., Stiehl, C., Eberhardt, R., Tünnermann, A., 2010, Submicron accuracy optimization for laser beam soldering processes, *Proc. SPIE 7585*, 758505.

Beckert, E., Wippermann, F., Walther, S., Burkhardt, T., Messerschmidt, B., Bartnitzek, T., Vahrenkamp, T., Eberhardt, R., Gäbler, D., Tünnermann, A., 2011, Autoclaveable miniaturized video endoscopes with simplified flip-chip assembly, *Proc. SPIE 7893*, 78930B.

Burkhardt, T., Mohaupt, M., Hornaff, M., Zaage, B., Beckert, E., Döring, H.-J., Slodowski, M., Reimer, K., Witt, M., Eberhardt, R., Tünnermann, A., 2011, Packaging Technology of Multi Deflection Arrays for Multi-Shaped Beam Lithography, *Proc. of IMAPS 44th International Symposium on Microelectronics*.

Burkhardt, T., Hornaff, M., Kamm, A., Burkhardt, D., Schmidt, E., Beckert, E., Eberhardt, R., Tünnermann, A., 2015, Low-strain laser-based solder joining of mounted lenses, *Proc. SPIE 9574*, 9574-21.

Escudero-Sanz, I., Ahlers, B., Bazalgette Courrèges-Lacoste, G., 2008, Optical design of a combined raman–laser-induced-breakdown-spectroscopy instrument for the european space agency exomars mission, *Opt. Eng.*, vol. 47, no. 3, pp. 033001-1–03301-11 .

Ribes, P., Burkhardt, T., Hornaff, M., Kousar, S., Burkhardt, D., Beckert, E., Gilaberte, M., Guilhot, D., Montes, D., Galan, M., Ferrando, S., Laudisio, M., Belenguer, T., Ibarmia, S., Gallego, P., Rodriguez, J. A., Eberhardt, R., Tünnermann, A., 2015, Solderjet bumping technique used to manufacture a compact and robust green solid-state laser, *Proc. SPIE 9520*, 952009.

Richter, L., Carianni, P., Durrant, S., Hofmann, P., Mühlbauer, Q., Musso, F., Paul, R., Redlich, D., 2015, Progress Report on Development of the Exomars 2018 Sample Processing and Distribution Subsystem (SPDS) and related OHB Sample Handling Studies, *Astra 2015 ESTEC*.

Rull Pérez, F., Martinez-Frias, J., 2006, Raman spectroscopy goes to Mars, *Spectroscopy Europe*, vol. 18, pp. 18–21.

Sansano, A., Navarro, R, Lopez-Reyes, G., Rull, F., 2014, Development of the Calibration Target for ExoMars' Raman Instrument (RLS), *45th Lunar and Planetary Science Conference.*